Available online at www.sciencedirect.com
SCIENCE DIRECT
Intermetallics 14 (2006) 1276–1290
Intermetallics
www.elsevier.com/locate/intermet

Assessment of the Fe–Ni–Al system

Luiz Eleno [a,*], Karin Frisk [b], André Schneider [c,1]

[a] Department of Materials Technology, Max Planck Institute for Iron Research, Max-Planck-Straße 1, 40237 Düsseldorf, Germany
[b] Computational Thermodynamics Research Group, Swedish Corrosion and Metals Research Institute, Drottning Kristinas väg 48, 114 28 Stockholm, Sweden
[c] Salzgitter Mannesmann Forschung GmbH, Metallurgy & Material Development, Head of Materials Technology Department, Ehinger Straße 200, 47259 Duisburg, Germany

Received 5 September 2005; accepted 9 November 2005
Available online 4 April 2006

Abstract

For the present assessment, the available experimental data from the literature on the Fe–Ni–Al system was reviewed, to provide reliable information for application- and alloy development-oriented purposes and for a future thermodynamic modelling of the system. The data consists of phase relationships and phase boundaries in the ternary system, as well as thermochemical and diffusion (both experimental and ab initio) results. The present status of the modelling of the system, following the Calphad formalism as well as other approaches, is also described.

Keywords: A. Intermetallics, miscellaneous; B. Order/disorder transformations; C. Phase diagrams; D. Site occupancy; E. Phase diagram, prediction

1. Introduction

In the last decades, much basic and applied research has been dedicated to intermetallic alloys (for reviews, see Sauthoff [1,2]). The wide range of applications of this specific set of materials ensures a continuous and prolific interest from the academic and industrial communities.

Alloys based on the Ni–Al binary system are one of the most important and employed classes of intermetallic materials. Due to the increase in ductility it provides, the well-known γ (disordered fcc)/γ′ (ordered $L1_2$-type) combination, for instance, builds up a starting point for the development of Ni-base super-alloys [3]. Another example is the thermoelastic martensitic transition β (B2) → β′ ($L1_0$), which is the basis for Ni-base shape-memory alloys [4–6].

Due to their good magnetic properties, Fe–Ni–Al alloys have been employed as the basis of the Alnico permanent magnets [7–9]. Later on, they were improved by major additions of Co and minor additions of Cu, Ti and traces of other elements [8].

Finally, the B2-NiAl ordered phase is of great interest in the development of high-temperature materials, due to its high melting point (∼1680 °C) [10,11] and excellent oxidation resistance, though it is brittle at room temperature [1]. This problem can be circumvented with the addition of disordered Fe-rich α (disordered bcc) and γ (disordered fcc) phases [3]. Alloy development based on this concept has been carried out through alloying with Cr (∼8 at%) and micro-alloying with Hf (∼0.1 at%), showing very promising properties for applications in industrial furnaces and petrochemical plants [2].

Although there is a vast number of potential applications for Fe–Ni–Al based alloys, the phase diagram knowledge is somewhat restricted to low Al contents (<50 at%), and even the best known region of the phase diagram shows some inconsistencies in the published information available. The α-Fe + B2-(Fe, Ni)Al miscibility gap, for instance, and its equilibrium with the fcc γ-(Fe,Ni) phase, is not established with sufficient accuracy at high temperatures (800–1100 °C). Considering the equally important γ/γ′ transition, the large disparity in the equilibrium data is striking, as noticed in the Ni_3Al–Ni_3Fe vertical section, and as further detailed in Section 2.4.2 (see Fig. 8).

* Corresponding author.
E-mail address: eleno@mpie.de (L. Eleno).
[1] Formerly at the Max Planck Institute for Iron Research, Düsseldorf, Germany.

0966-9795/$ - see front matter © 2006 Elsevier Ltd. All rights reserved.
doi:10.1016/j.intermet.2005.11.021

The Fe–Ni–Al system has been previously reviewed by Rivlin and Raynor [12]. The same authors made further emendations in 1988 [13]. Budberg and Prince [14] have updated the state of knowledge of the system in 1992. Since then new experimental information has been generated and should now be reviewed, though short literature updates were published recently by Raghavan [15,16].

The present assessment has therefore three main objectives. The first is to critically evaluate the available thermodynamic information on the Fe–Ni–Al ternary system, including the whole compositional range. For that, the literature published on the system has been compared and analysed, the results of which are presented in the following sections. The second objective is to detect regions of the phase diagram where scanty information is at hand, thus suggesting new experimental work. Lastly, the data collected in the present assessment should serve as a starting reference for future thermodynamic modelling and optimisation of thermochemical databases.

The organisation of the present work is as follows: phase relationships and phase transitions are discussed in Section 2, including a description of the phases present in the binaries and in the ternary systems. Thermochemical data (formation enthalpies, activities) are described in Section 3. Atomistic (site-preference occupation and vacancy formation) and diffusion data are given in Section 4. Finally, the present status of Calphad-type modelling and calculations following other formalisms will be described in Section 5.

2. Phase diagram data

All solid phases present in the Fe–Ni–Al system are described in Table 1. A partial list of invariant reactions is found in Table 2. The invariant reaction temperatures for the Fe–Al and Fe–Ni binary systems were taken from the binary reviews, references to which are given in Table 1. For the Ni–Al system, the data from Hilpert et al. [17] was employed. The ternary reactions were taken from several references, but are based on the reviews of Rivlin and Raynor [12,13] and especially Budberg and Prince [14]. The speculations of Prince [18] provide a good overall description of the reaction scheme for $x_{Al} > 0.6$, although they lack more detailed information, particularly regarding some transition temperatures.

Throughout this work, second-order phase boundaries will be indicated by hatched lines and magnetic transitions by dash-dotted ones. When uncertainties with respect to phase boundaries exist, they will be indicated by dashed lines. When even this is not possible, the region will be labelled with a question mark. In isothermal sections, three-phase fields will be coloured grey.

2.1. Binary subsystems and binary compounds

In this section we describe briefly the binary phase diagrams as published in the Massalski handbook [35], since they constitute one of the most widespread and employed compilations, specially for engineering purposes. No details will be given concerning possible disagreements and controversies, except when they are important to the ternary system. This is the case for the melting temperature of Ni–50 at% Al (B2), for instance, which influences the rendering of the liquidus projection. The solubility of the third element into the ternary system at selected temperatures is given in Table 1. The articles by Palm and Lacaze and by Cacciamani et al. in this special issue update the information available on the Fe–Al and Fe–Ni systems, respectively.

2.1.1. Fe–Al

The Fe–Al phase diagram according to Kattner [36] is shown in Fig. 1a. The Fe-rich portion of the phase diagram is dominated by the A2 → B2 and (A2 or B2) → $D0_3$ ordering reactions in the bcc lattice. Some authors [37] further divide the B2-FeAl field into three different zones, together with a low-temperature region within the A2 stability range, the so-called *K*-state. The latter feature is supported by a recent work of Ikeda et al. [38].

For $x_{Al} > 0.5$ several intermetallic phases are stabilised. There are still some inaccuracies concerning this part of the phase diagram, namely, the structure of the ε phase and the stability range of the $FeAl_2$, Fe_2Al_5 and Fe_4Al_{13} phases.

The structure of the ε phase is not yet known with certainty, due to the fact that it decomposes spontaneously during cooling. Taylor and Jones [39] first suggested that it could be either orthorhombic or hexagonal (*hR*78, $R\bar{3}18$, $D8_{10}$, Al_8Cr_5), the latter hypothesis being supported by investigations on different ternary systems, namely, Fe–Al–Cr [40], Fe–Al–Ti [41], and Fe–Al–Mo [42]. The structure given in Table 1 is, however, not to be taken as conclusive.

Seierstein [43] presented the most recent thermodynamic modelling of the Fe–Al system. For a description of the magnetic and chemical ordering the evaluation of Ohnuma et al. [44] can be combined with that of Seierstein's. The calculated phase diagram using these two descriptions is shown in Fig. 1b.

2.1.2. Ni–Al

Fig. 2a shows the Ni–Al phase diagram according to Singleton et al. [45]. The melting temperature of the equiatomic NiAl (B2) phase, according to these authors, is situated at 1638 °C, which is about 40 °C lower than reported in more recent works. By DTA measurements, Bitterlich et al. [10] gave 1681 °C as the melting temperature, and Rablbauer et al. [11] found the same at 1674 °C. Both experiments also confirm the calculations of Ansara et al. [46] and Dupin et al. [47], according to whom the melting temperature should be 1678 °C.

There are also discrepancies concerning the solidification reactions in the Ni-rich side. According to Hilpert et al. [17], the reactions among the liquid and the γ-Ni, the γ′-$AlNi_3$ ($L1_2$) and NiAl (B2) phases occur first peritectically following the reaction $L + \gamma\text{-Ni} \rightarrow \gamma\text{-}AlNi_3$ ($L1_2$) at 1372 °C, proceeding then to the eutectic $L \rightarrow AlNi$ (B2) + γ′-$AlNi_3$ ($L1_2$) at 1369 °C. According to Singleton et al. [45], on the other hand, the first peritectic reaction occurs at 1395 °C, $L + AlNi$ (B2) → $\gamma' - AlNi_3(L1_2)$, the liquid composition advancing then to the eutectic $L \rightarrow \gamma\text{-Ni} + \gamma'\text{-}AlNi_3(L1_2)$ at 1385 °C. The agreement between experimental information

Table 1
Solid phases in the Fe–Ni–Al system

Phase[a]	Pearson symbol	Space group	Strukturbericht designation	Prototype	Composition range[b]	Solubility of 3rd element	Lattice parameters
Fe–Al					at% Al	at% Ni	(Å)
α-Fe, δ-Fe	*cI*2	$Im\bar{3}m$	A2	W	0 to ~45	~20	0–25 at% Al: 2.867–2.911 [19]
γ-Fe	*cF*4	$Fm\bar{3}m$	A1	Cu	0–1.3	100	
Fe_3Al ($D0_3$)	*cF*16	$Fm\bar{3}m$	$D0_3$	BiF_3	~23 to ~34		5.790 [20]
FeAl (B2)	*cP*2	$Pm\bar{3}m$	B2	CsCl	23.3 to ~55	100	2.907 [21]
ε[c]	*hR*26	–	–	Al_8Cr_5	~58 to ~65		
$FeAl_2$	*aP*18	P1	–	Al_2Fe	66–66.9	~3	$a = 4.878$, $b = 6.461$, $c = 8.7476$ [22] $\alpha = 87.927°, \beta = 74.452°, \gamma = 83.11°$
Fe_2Al_5	*oC*16	*Cmcm*	–	–	70–73	~2	
Fe_4Al_{13}	*mC*102	*C*2/*m*	–	–	74.5–76.6	~7	$a = 15.492$, $b = 8.078$, $c = 12.471$, $\beta = 107.66°$ [23]
(Al)	*cF*4	$Fm\bar{3}m$	A1	Cu	~100		
Ni–Al					at% Al	at% Fe	(Å)
γ-Ni	*cF*4	$Fm\bar{3}m$	A1	Cu	0–21.2	100	3.5486 [24]
γ′-Ni_3 Al	*cP*4	$Pm\bar{3}m$	$L1_2$	Cu_3Au	24–27	~15	3.5695 [24]
Ni_5Al_3	*oC*16	*Cmmm*	Ga_3Pt_5	–	~32–36		
NiAl (B2)	*cP*2	$Pm\bar{3}m$	B2	CsCl	30.8–58	100	2.877 [25]
Ni_2Al_3	*hP*5	$P\bar{3}m1$	$D5_{13}$	Al_3Ni_2	59.5–63.2	~4	57–60 at% Al: $a = 4.442$–4.036, $c = 4.895$–4.915 [26] 60–23 at% Al: $a = 4.036$–4.053, $c = 4.895$–4.902
$NiAl_3$	*oP*16	*Pnma*	$D0_{11}$	Fe_3C	~23–26		$a = 6.5982$, $b = 7.3515$, $c = 4.8021$ [27]
(Al)	*cF*4	$Fm\bar{3}m$	A1	Cu	99.89–100	~2	4.025 [28]
Fe–Ni					at% Ni	at% Al	(Å)
α-Fe	*cI*2	$Im\bar{3}m$	A2	W	0–5.5	40	2.860 [29]
δ-Fe	*cI*2	$Im\bar{3}m$	A2	W	0–3.5		
γ-(Fe,Ni)	*cF*4	$Fm\bar{3}m$	A1	Cu	0–100	1.95	3.587 [29]
γ′-$FeNi_3$	*cP*4	*eq*14	$L1_2$	$AuCu_3$	63–85	~12	3.5550 [30]
Al–Fe–Ni					at% Al	at% Ni	(Å)
Al_9FeNi	*mP*22	$P2_1/c$	$D8_d$	Al_9Co_2	82–83	7–14	$a = 8.598$, $b = 6.271$, $c = 6.207$, $\beta = 94.76°$ [31]
$Al_{10}Fe_3Ni$	*hP*28	$P6_3/mmc$	$D8_{11}$	Al_5Co_2	70–73	55–60	
$Al_{10}FeNi_3$?[d]	–	–	–	–	–	–	

For the sake of clarity, some entries are shown repeatedly in the different binary systems.
[a] The phase designation adopted here does not necessarily correspond to those found in the literature, mainly because there is no general agreement in this regard.
[b] In the binary system.
[c] The structure of the high-temperature ε phase, which could be Al_8Cr_5, has not yet been settled.
[d] This phase has been reported by Khaidar et al. [31], and is only stable in a narrow temperature range (~800 –900 °C). A quasi-crystalline phase with composition $Al_{71.6}Fe_{5.4}Ni_{23.0}$ has also been reported by Lemmerz et al. [32], Grushko et al. [33], and Lemmerz [34] and was found to be stable from 847 °C to 930 °C.

and the diagram of Singleton et al. [45] is not sufficient in the Ni-rich side at higher temperatures, as the authors themselves state in their work. For this reason, Table 2 shows the data taken from Hilpert et al. [17] for the Ni–Al binary system. The data of these authors also agree considerably well with the results of Bremer et al. [48] (within an estimated error of 5 °C). Another important feature that the publications of Bremer et al. [48] and Hilpert et al. [17] share in common is the fact that the temperature difference between the peritectic and eutectic invariants is very small (ca. 3 °C), differing from previous results, which give it at about 10 °C and/or change the reaction sequence, as is the case for the data of Singleton et al. [45].

According to Ellner et al. [49], there exists a low-temperature phase, with stoichiometry given by Ni_3Al_4, forming peritectoidically from the B2-NiAl and the Ni_2Al_3 phases. The transition temperature was found to be 580 °C. The structure of the Ni_3Al_4 phase was determined by X-ray diffraction to be iso-typical to the Ga_4Ni_3 prototype (*cI*112, $Ia\bar{3}d$), and shows vacancy ordering in different sublattices. Nevertheless, this phase is not included in the phase diagrams showed in the present work, since it was also plotted in dashed lines in the original reference.

The most recent Calphad evaluation of the Ni–Al system was presented by Dupin et al. [47], who included all phases needed for the thermodynamic description of the ternary Cr–Ni–Al system. The calculated Ni–Al phase diagram according to Dupin et al. [47] is shown in Fig. 2b.

2.1.3. Fe–Ni

Fig. 3(a) presents the Fe–Ni phase diagram, based on the work of Swartzendruber et al. [50]. Nickel forms with iron

Table 2
Invariant reactions in the Fe–Ni–Al system

Fe–Al	Fe–Ni	Fe–Ni–Al	Ni–Al
	p_1 1514 °C $L + \delta\text{-Fe} \rightarrow \gamma\text{-(Fe,Ni)}$		
			p_2 1372 °C $L + \gamma\text{-Ni} \rightarrow \gamma'\text{-}Ni_3Al$
			e_1 1369 °C $L \rightarrow$ NiAl (B2) + $\gamma'\text{-}Ni_3Al$
		U_1 ~1365 °C $L + \gamma' \rightarrow \gamma\text{-(Fe,Ni)} +$ B2-(Fe,Ni)Al	
		e_2 1340 °C $L \rightarrow \gamma\text{-(Fe,Ni)} +$ B2-(Fe,Ni)Al	
p_3 1232 °C $L + \alpha\text{-Fe} \rightarrow \varepsilon$			
e_3 1165 °C $L \rightarrow \varepsilon + Fe_2Al_5$			
p_4 ~1160 °C $L + Fe_2Al_5 \rightarrow Fe_4Al_{13}$ p_5 1156 °C $\varepsilon + Fe_2Al_5 \rightarrow FeAl_2$			
			p_6 1133 °C $L + \text{NiAl(B2)} \rightarrow Ni_2Al_3$
e_4 1102 °C $\varepsilon \rightarrow$ FeAl (B2) + $FeAl_2$			
			p_7 854 °C $L + Ni_2Al_3 \rightarrow NiAl_3$
		U_2 840 °C $L + Ni_2Al_3 \rightarrow NiAl_3 + Fe_4Al_{13}$ P 809 °C $L + Fe_4Al_{13} + NiAl_3 \rightarrow FeNiAl_9$	
e_5 655 °C $L \rightarrow Fe_4Al_{13} + \text{(Al)}$			
		U_3 650 °C $L + Fe_4Al_{13} \rightarrow FeNiAl_9 + \text{(Al)}$	
			e_6 640 °C $L \rightarrow NiAl_3 +$ (Al)
		E 638 °C $L \rightarrow \text{(Al)} + NiAl_3 + FeNiAl_9$	

The list is not exhaustive; for a more complete — though speculative — account, see Prince [18].

a disordered fcc solid solution encompassing the whole compositional range, here designated by γ-(Fe,Ni). At lower temperatures (below ~500 °C) the ordering transition γ-(Fe,Ni) → γ′-$FeNi_3$ ($L1_2$) takes place.

The thermodynamic description of the Fe–Ni system by Dinsdale and Chart [51] was revised by Lee [53], and works well at high temperatures. At lower temperatures, however, ordering reactions occur, which are essential for the ternary Fe–Ni–Al system. This part of the diagram was described by Ansara [52]. The resulting phase diagram is given in Fig. 3(b).

2.2. Ternary compounds

There are reportedly two ternary crystalline phases in the Fe–Ni–Al system. The monoclinic $FeNiAl_9$ phase forms peritectically at 809 °C [31], according to the reaction $L + Fe_4Al_{13} + NiAl_3 \rightarrow FeNiAl_9$, and shows a very narrow homogeneity range (82–83 at% Al, 7–14 at% Ni). At lower temperatures, there are further reactions including the $FeNiAl_9$ phase, which can be seen in Table 2.

The Fe_3NiAl_{10} phase forms at a temperature slightly above 1050 °C [16,31], according to $L + Fe_3NiAl_{10} \rightarrow Ni_2Al_3 + Fe_4Al_{13}$. The $FeNiAl_5$ phase described by Ellner and Röhrer [54] can be supposed to be within the stability range of Fe_3NiAl_{10} [14], which is about 70–73 at% Al, 55–60 at% Ni. According to Bradley and Taylor [55], this phase has a hexagonal structure, but the X-ray experiments performed by Khaidar et al. [31] show a large number of reflections that could not be indexed by that assumption. The true lattice for the Fe_3NiAl_{10} phase remains therefore unclear.

Using DTA measurements, Khaidar et al. [31] found a possible new ternary phase, which was assumed to be $FeNi_3Al_{10}$, stable at temperatures around 900–850 °C. Due to the fact that this phase decomposes during slow cooling, the authors could not identify its structure. More recently, a quasi-crystalline decagonal phase [32–34,56,57] was found to form at compositions very close to those studied by Khaidar et al. [31]. The stoichiometry of this phase was given as $Fe_{5.4}Ni_{23.0}Al_{71.6}$, being stable from 930 °C to 847 °C [34]. Recently, Grushko and Velikanova [58] published a review on quasi-crystalline phases in several ternary alloys of aluminium with transition metals. The authors discuss the stability of this type of structure and argue that they can be stable in the same sense (sic) as periodic (or ''fully'' crystalline) phases in multi-component systems. The Al-rich corner of the isothermal section at 850 °C, shown in Fig. 6f, presents the phase equilibria involving the quasi-crystalline phase [32–34] (although indicated in the figure as $FeNi_3Al_{10}$ followed by a question mark). The authors employed X-ray analysis and transmission electron microscopy to ascertain their results on several samples annealed at 850 °C for 68 h and subsequently water-quenched. More recently, however, de Laissardiere et al. [59] asserted in a review paper that decagonal quasi-crystals in the Fe–Ni–Al system are to be regarded as metastable.

2.3. Liquidus projection

A partial liquidus projection, for temperatures ranging from 1250 °C to ~1680 °C is given in Fig. 4a [13]. It should be noted that only some of the troughs are depicted. In the centre of the diagram, for instance, the reactions involving the

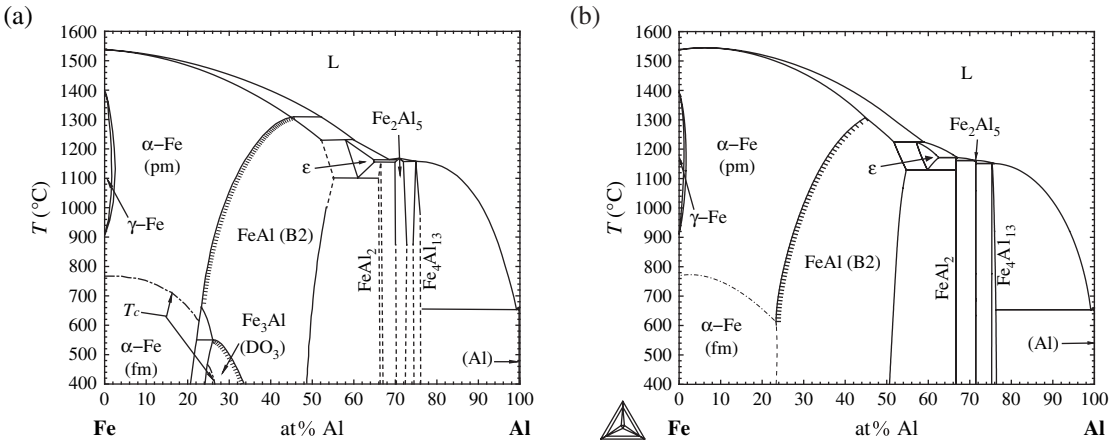

Fig. 1. (a) Binary subsystem Fe–Al [36]. (b) Calculated binary Fe–Al phase diagram [43,44]. The two-sublattice model used to describe the bcc phases does not allow the modelling of the $D0_3$ structure. The second-order boundary is represented by hatched lines, while the magnetic transition is depicted with dash-dotted lines.

Fe_3NiAl_{10} phase cannot be represented due to the lack of information. The e_2 reaction occurs at a minimum of the trough, around 1340 °C, but the exact composition of the phases involved in this reaction is not known.

Close to the Ni–Al binary and up to 20 at% Ni, the liquidus troughs can be drawn for low temperatures (<840 °C), as shown in Fig. 4b [13]. Due to the restricted homogeneity range of the $FeNiAl_9$ phase, the position of the P reaction $L + Fe_4Al_{13} + NiAl_3 \rightarrow FeNiAl_9$ (809 °C) could be identified with some accuracy. The liquidus projection was determined by Phillips [61] for very high Al concentrations ($x_{Al} \gtrsim 0.97$) and for temperatures in the range 645–720 °C.

It is also worth mentioning in this paragraph a vertical section of the solidus surface from NiAl to FeAl, taken from Bitterlich et al. [10] and given in Fig. 5. For comparison, the data from Bradley [60] is plotted in the same diagram. The main discrepancy is the maximum at the NiAl side, which is equivalent to the melting point of the NiAl (B2) phase (see Fig. 2a and discussion in Section 2.1.2). This leads consequently to a worse agreement in the region closer to the Ni–Al binary system with respect to the calculation described in Section 5.1.1.

2.4. Isothermal and isoplethal sections

The Fe–Ni–Al system can be quite suitably divided into three broad regions, namely the Fe-rich corner, where ordering in the bcc lattice takes place; the Ni-rich corner, with ordering in the fcc lattice; and the Al-rich corner and the appearance of ternary phases. In the subsections that follow, isothermal and isoplethal sections of the ternary phase diagram will be presented as a single unity whenever possible, but the discussion will be separated into these three different subjects for greater convenience and clarity.

2.4.1. Ordering in the bcc lattice

The miscibility gap on the bcc lattice between the disordered A2 phase and the ordered B2 phase has been thoroughly studied by Hao et al. [62], for temperatures ranging from 850 °C to 1150 °C, using diffusion couple experiments. Their results correspond to the Fe-rich corner of the isothermal sections presented in Fig. 6c–f. The equilibria with the disordered fcc phase closer to the Fe–Ni binary were also investigated by the same authors. When aging as-quenched Fe–4.1

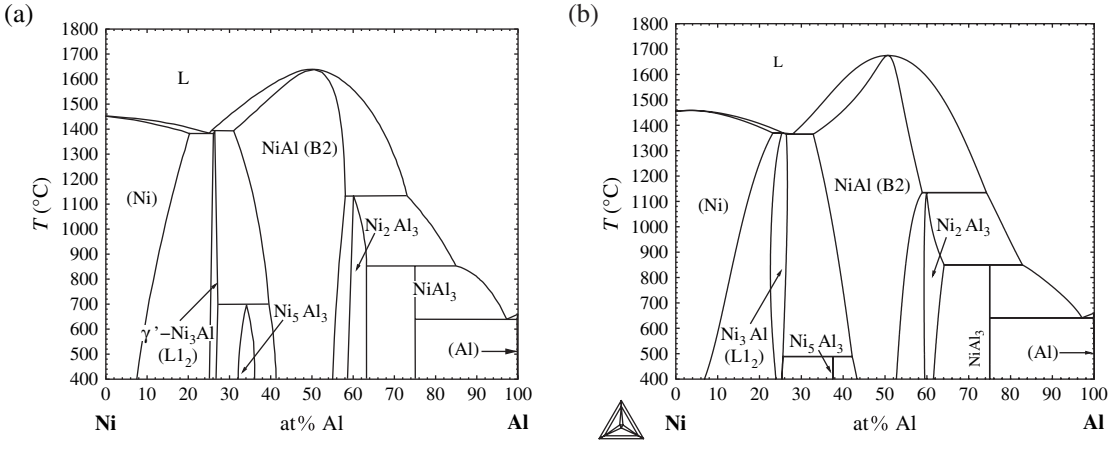

Fig. 2. (a) Binary subsystem Ni–Al [45]. (b) Calculated binary Ni–Al phase diagram [47].

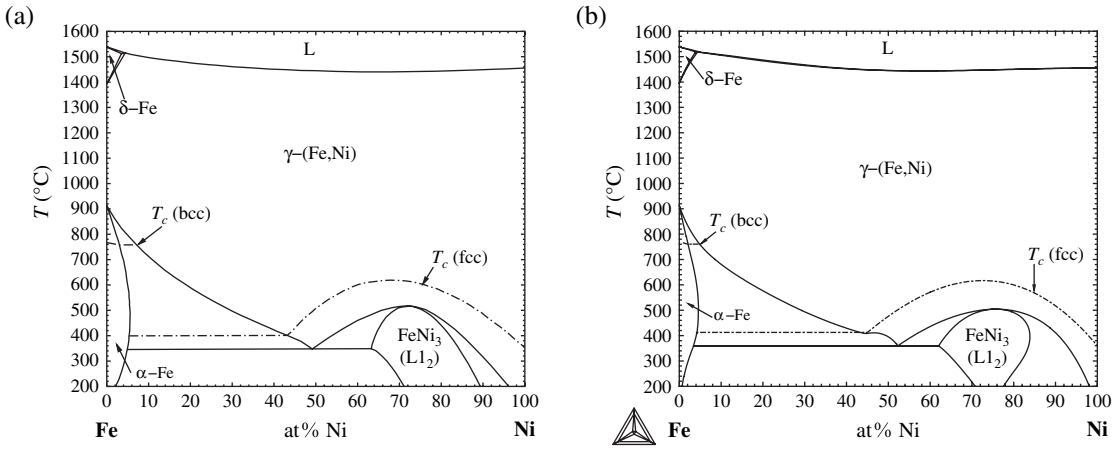

Fig. 3. (a) Binary subsystem Fe–Ni [50]. (b) Calculated binary Fe–Ni phase diagram [51,52].

at% Ni–23.2 at% Al samples at temperatures in the range 500–1050 °C, Liu et al. [64] found a reaction sequence that includes two B2 phases in equilibrium below ~725 °C, with partition of Ni and Al between them. This result, and whether it represents a true equilibrium state of the system or a kinetic feature, has still to be cross-checked independently in order to be confirmed.

The Fe-rich corner of the isotherms at 1350 °C and 1250 °C, shown in Fig. 6a and b, respectively, were taken from Bradley [60]. The same holds for the 750 °C isotherm, shown in Fig. 6g. The second-order phase boundaries, investigated by Hao et al. [62], are represented by hatched-full lines. In Fig. 6b (1250 °C) and g (750 °C), they have been extrapolated from the limiting binary Fe–Al system, and are thus shown in hatched-dashed lines. In drawing Fig. 6b, it was supposed that the second-order line does not open in a miscibility gap, following the indications that the miscibility gap vanishes above 1150 °C. In the Fe–Al binary at 1350 °C the B2 phase is not stable anymore; inside the ternary, on the other hand, there must still be an ordering reaction on the bcc lattice at that temperature, because the B2 phase melts around 1680 °C in the Ni–Al binary system, as already stated. For this reason, the central part of Fig. 6a is not known with certainty, regarding the A2 + B2 equilibrium at temperatures above 1350 °C. This transition could have a first- or second-order character, even though the latter is more likely, following the trend already presupposed at 1250 °C.

The isoplethal section from the Fe corner to NiAl is shown in Fig. 7a, constructed from data given by Marcon et al. [9] and Dannöhl [65], in which is shown the interaction between the γ-loop and the miscibility gap in the bcc lattice, creating the three-phase field shown in dashed lines. It should be noticed that the extent of this field, according to Dannöhl [65], is much greater (up to about 40 at% Fe) than that shown in Fig. 7a. This speculation is, however, not corroborated by the isothermal sections shown in Fig. 6c–g. The data from Marcon et al. [9] also generally confirm the results of Bradley [60], although they failed to notice the three-phase field that should exist in this part of the diagram (shown in dashed lines in Fig. 7a). Low-temperature data concerning the bcc miscibility gap were also given by Marcon and Lay [7]. One should be careful to notice that the solidus and liquidus lines present the

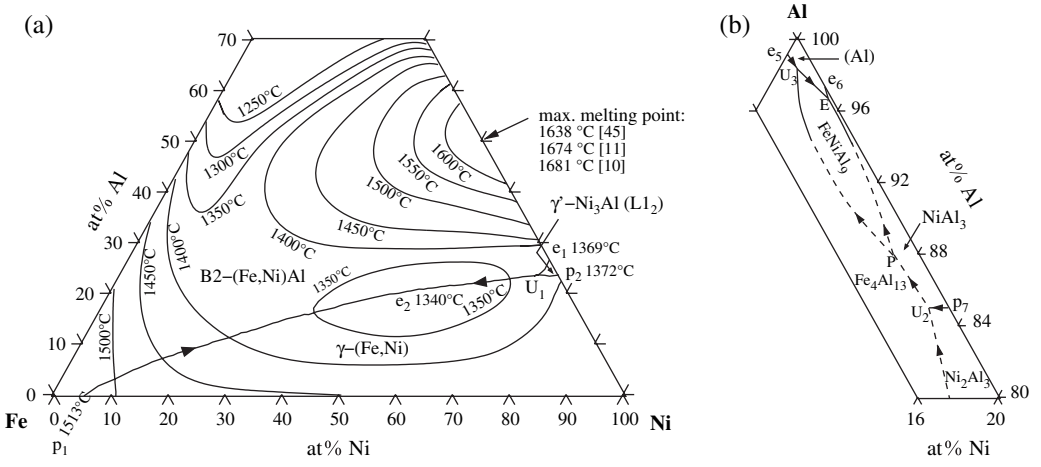

Fig. 4. (a) Partial liquidus surface with isotherms from 1250 °C to 1680 °C. [13,60]. (b) Liquidus troughs close to the Al corner [14].

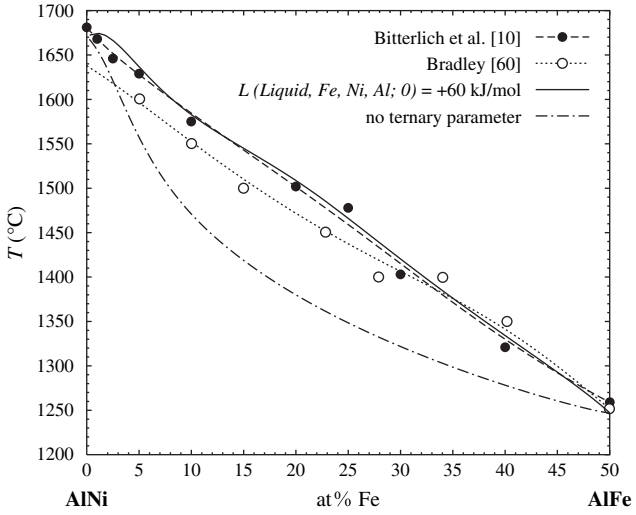

Fig. 5. Solidus temperatures in the section from NiAl to FeAl, according to Bitterlich et al. [10] (filled circles). The open circles correspond to the data of Bradley [60]. The full line is a trial-and-error fit to the Bitterlich et al. [10] data with the introduction of a ternary parameter, L(Liquid, Fe, Ni, Al;0) = +60 kJ/mol to a database with only binary interactions (see Section 5). The dash-dotted line indicates the calculation without this parameters.

problems discussed in Section 2.3, that is, the melting point at the NiAl side is about 40 °C lower than determined by more recent works [10,11]. It is very likely that this fact bears consequences also inside the ternary system.

Following Bradley and Taylor [55] and Bradley [55,60,63,66], Hao et al. [62] also constructed the isoplethal section shown in Fig. 7b, which is slightly away from the NiAl–Fe isopleth. It is interesting to notice in Fig. 7b that the γ-loop at the Fe side does not show up at all with the small additions of aluminium to the end-members of the pseudo-binary NiAl–Fe (Fig. 7a).

2.4.2. Ordering in the fcc lattice

In the Ni-rich corner, the ordering in the fcc lattice from the γ-Ni phase to the γ′-$AlNi_3$ ($L1_2$) phase takes place. The equilibrium between the fcc phases and the bcc ordered (B2) phase is also present in a wide temperature range. The main references for this part of the diagram are still the works by Bradley [60,63,66] with further contributions from other authors [67–73].

All the data from the authors cited in the last paragraph are incorporated into the isotherms shown in Fig. 6a–g. The general lines are those of Bradley [60], with further adjustments to match the boundaries found by Hao et al. [62] in the Fe-rich corner. The more recent work by Himuro et al. [73] also confirms the previous results.

The pseudo-binary section from Ni_3Al to Fe_3Al, shown in Fig. 8, gives an idea of the scattering of the data on this part of the diagram, mainly with respect to the γ′-Ni_3Al ($L1_2$)/γ-Ni + γ′-Ni_3Al ($L1_2$) phase boundary. In particular, the data of Goman'kov et al. [70] is in marked disagreement with those of the other authors. The EPMA results of Jia et al. [72] seem to be those with greater agreement between each other. But the 70 °C difference in the measurement of the alloy with approximately 7 at% Fe is still to be noticed. One has to pay attention to the fact that the EPMA results that are plotted in the pseudo-binary are merely extrapolations from measurements in different sections, because obviously the tie-lines determined from a diffusion couple or equilibration experiment do not necessarily lie on the isopleth. It is possible then to assert that the DTA measurements are more precise in the case of this experiment, since what is plotted in the vertical section is actually what was measured, viz., the temperature of beginning and end of the two-phase field for one particular composition.

For this vertical section, the phase diagram update of Raghavan [16] adopts the lines from Masahashi et al. [67]. Raghavan also considered the previous data of Bradley [60] and the results derived from different experimental techniques employed by Masahashi et al. [67]. For the γ′-Ni_3Al ($L1_2$)/γ-Ni + γ′-Ni_3Al ($L1_2$) transition, the large scattering of data points suggest the inadequacy of some of the techniques and extrapolations for the drawing of this vertical section. It seems that the sluggishness of the reaction and the small size of the precipitates are a severe hindrance to equilibrium determination (the difficulty in the determination of the γ′-Ni_3Al ($L1_2$)/γ-Ni + γ′-Ni_3Al ($L1_2$) boundary is also present in the binary Ni–Al, as examined by Ma and Ardell [74]). On the other hand, the EPMA results of Masahashi et al. [67] (indicated with upward triangles in Fig. 8) are in good agreement with those of Jia et al. [69], and also with the DTA ones from Himuro et al. [72]. Therefore, the EPMA data of Masahashi et al. [67] and Jia et al. [69], and the DTA results of Himuro et al. [72] were considered as the critical experiments for this vertical section, and the dash-dotted line in Fig. 8 can be taken as a reasonable fit to these data.

2.4.3. Al-rich corner and ternary phases

The Al-rich corner of the phase diagram was investigated by Khaidar et al. [31], who determined Al-rich isothermal sections at 1050 °C, 950 °C and 750 °C, which were considered to draw Fig. 6d, e and g, respectively. The 850 °C isotherm was not accomplished due to the interference of the $FeNi_3Al_{10}$ phase in the DTA signal. A small part of this isotherm (0–20 at% Fe, 60–80 at% Al) was later investigated by Lemmerz et al. [32–34], in order to describe the equilibria involving the decagonal quasi-crystalline phase. The authors provided the phase equilibria of this phase at 850 °C, which were incorporated in Fig. 6f of the present work.

The isotherms shown in Fig. 6(d), (e) and (g) were corrected using data from the binaries Fe–Al and Ni–Al, also following the update of Raghavan [16]. It should be noted that the 750 °C isotherm is not complete, being valid only for $x_{Al} \gtrsim 0.75$ and $x_{Al} < 0.5$. The isotherms at 1050 °C and 950 °C confirm the results of Bradley and Taylor [55].

Budberg and Prince [14] accepted an isotherm at 620 °C on the Al-rich-corner ($x_{Al} > 0.75$), taken from Schrader and Hanemann [75]. At this temperature, the liquid phase is already totally consumed, and the equilibria now involve the (Al) terminal phase (Fig. 9).

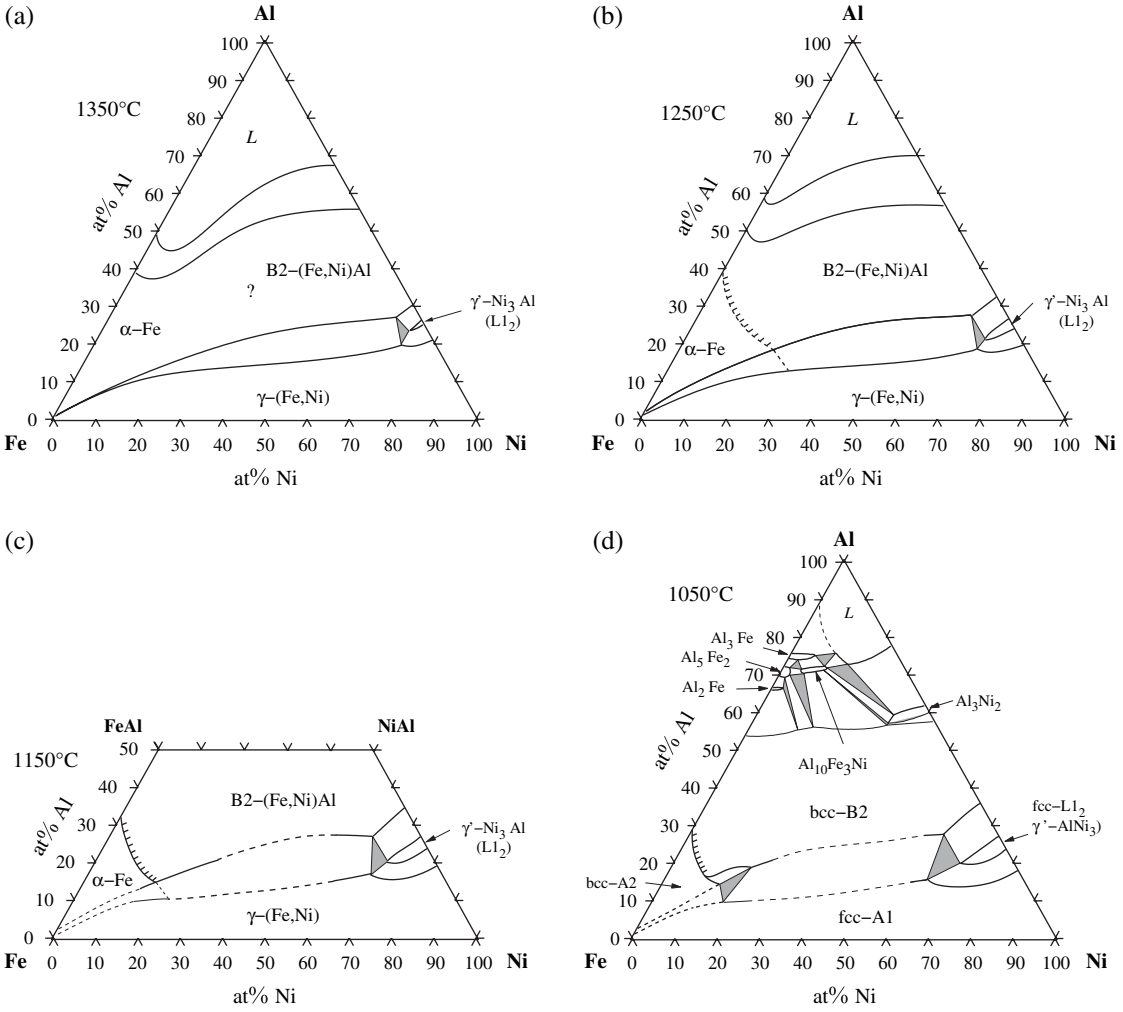

Fig. 6. (a) Isothermal section of the Fe–Ni–Al phase diagram at 1350 °C [55,60]. The α-Fe + B2 field (or second-order line) that should exist in the centre of the diagram has not been investigated. (b) Isothermal section of the Fe–Ni–Al phase diagram at 1250 °C [55,60]. (c) Isothermal section of the Fe–Ni–Al phase diagram at 1150 °C [55,60,62]. (d) Part of the isothermal section of the Fe–Ni–Al phase diagram at 1050 °C [16,31,60,62]. (e) Isothermal section of the Fe–Ni–Al phase diagram at 950 °C [16,31,60,62]. (f) Isothermal section of the Fe–Ni–Al phase diagram at 850 °C [16,31,60,62]. The equilibria of the quasi-crystalline phase $FeNi_3Al_{10}$ (?) at 850 °C [32–34] is also shown. (g) Fe–Ni–Al phase diagram at 750 °C [16,31,60,62,63]. The central area of the isotherm has not been investigated.

3. Thermochemical data

3.1. Experimental

Activity measurements in binary Fe–Al and Ni–Al B2 alloys have been carried out by Raj et al. [76], in the range 1140–1600 K (867–1327 °C) and 1178–1574 K (905–1301 °C), respectively. The integral enthalpies and entropies of mixing were found to be almost temperature independent, with large and negative mixing entropies. Further results for the B2-NiAl phase were later presented by Bencze et al. [77], including calculations of the thermodynamic factor for diffusion.

Enthalpies of formation of B2 $Fe_{1-x}Al_x$ and B2 $(Ni,Fe)_{1-x}Al_x$ were determined by Grün et al. [78] and Breuer et al. [79] at 1073 K (800 °C). Their results for the ternary alloys are shown in Fig. 10. It is clear that off-stoichiometry deviations tend to destabilise the ordered B2 structure and also to increase the deviation with respect to the mechanical mixture line (dashed lines in the Figure). Substitution of Fe by Ni, while keeping the Al content constant, leads to an increasingly negative enthalpy of formation. Zubkov et al. [80] determined standard enthalpies of formation (ΔH_f°, 298^o) of three ternary B2 alloys with Fe contents up to 5 at%. Their results show some deviations with respect to the data of Grün et al. [78] and Breuer et al. [79].

For very low Al contents, Li et al. [81] determined Al activities and interaction coefficient of Al in Ni for liquid alloys at 1873 K (1600 °C). The composition ranges of the samples were 15–27.7 at% Ni and 42 ppm Al to 0.017 at% Al (plus Fe). Ostrovskii et al. [82] determined the heat of solution of Al in Fe–Ni–Al liquid alloys at ~1600 °C for several compositions covering practically the whole composition range.

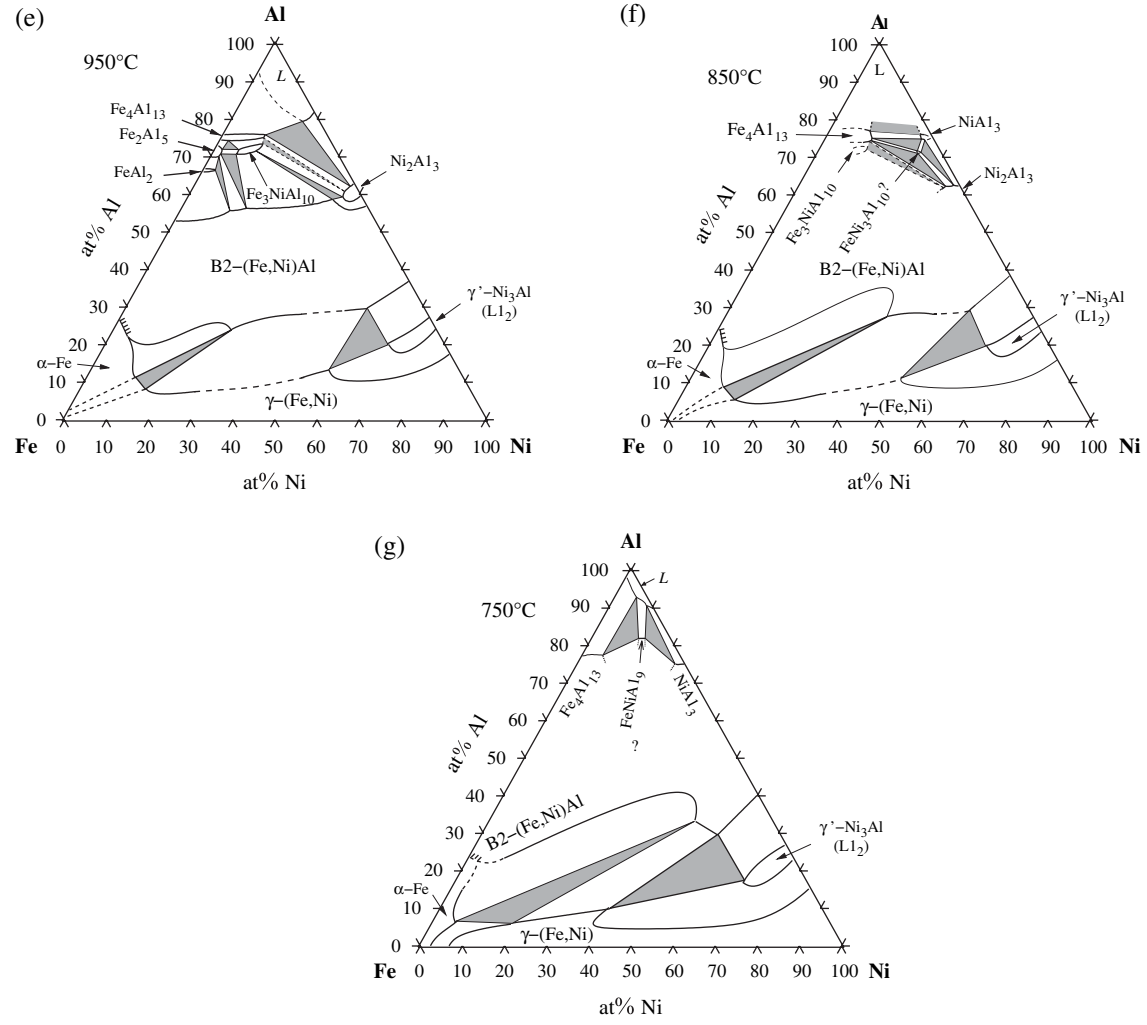

Fig. 6 (*continued*).

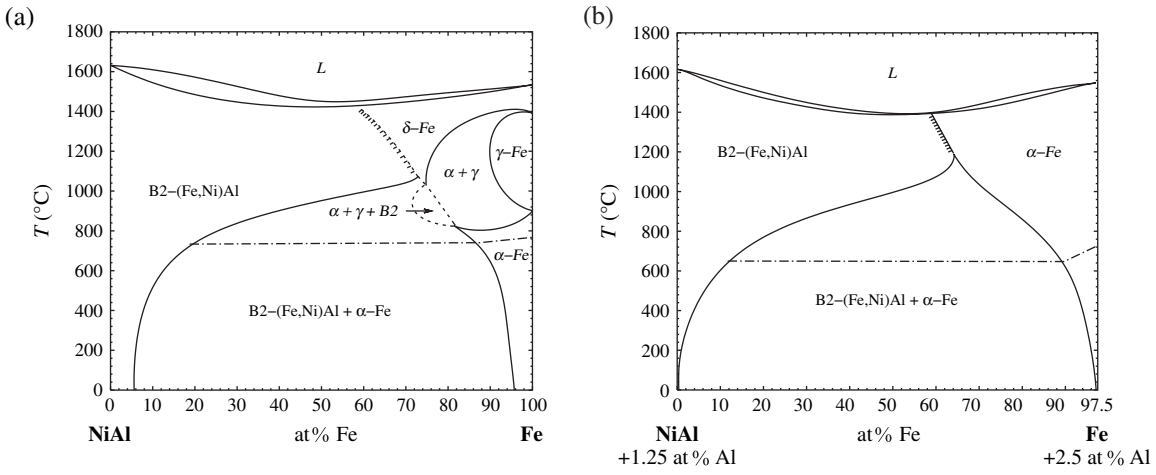

Fig. 7. (a) Pseudo-binary phase diagram from NiAl to Fe: miscibility gap between ordered (B2) and disordered (α-Fe) bcc phases and relationships with the $\alpha - Fe + \gamma - Fe$ field [9,63,65]. (b) Pseudo-binary phase diagram from $Ni_{48.75}Al_{51.25}$ to $Fe_{97.5}Al_{2.5}$: miscibility gap between ordered (B2) and disordered (α-Fe) bcc phases [55,62].

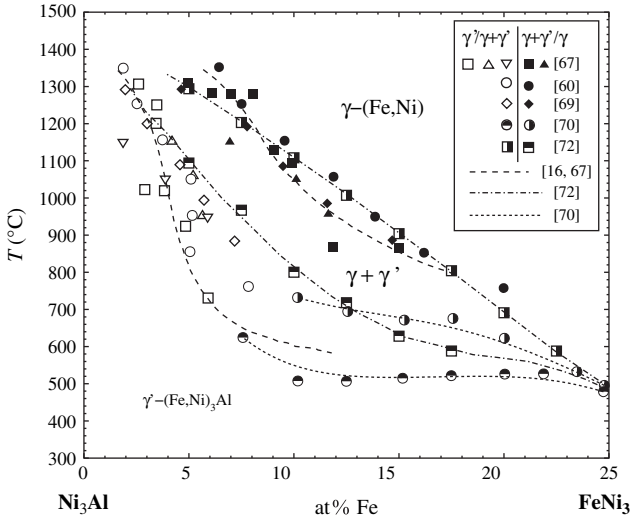

Fig. 8. Vertical section of the Fe–Ni–Al phase diagram from Ni_3Al to $FeNi_3$ [16,60,67,69,70,72]. The data points are shown to indicate the level of uncertainty on this part of the phase diagram. The broken lines give an idea of the different interpretations for the phase boundaries, according to some of the authors. Notice that melting of Ni_3Al occurs at about 1400 °C.

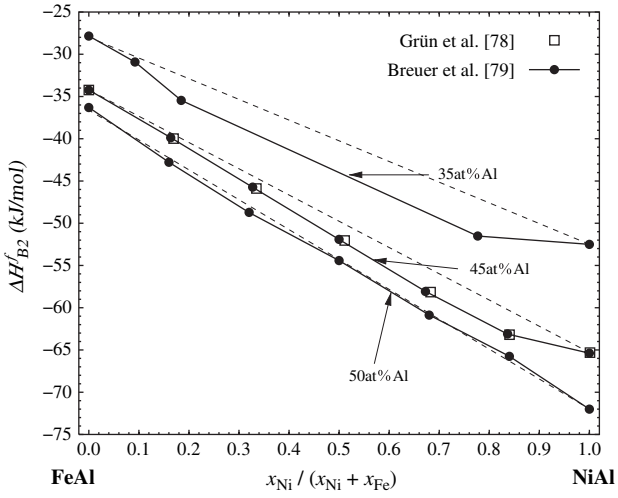

Fig. 10. Enthalpy of formation of B2-(Fe,Ni)Al for several compositions at 1073 K (800 °C). According to Grün et al. [79]. Reference state: bcc Fe, fcc Ni, and liquid Al at 1073 K. The dashed lines represent the mechanical mixture of the end-members (i.e., B2-FeAl and B2-NiAl).

Albers et al. [83] determined activities and partial enthalpies of mixing from 1304 K (1031 °C) to 1698 K (1425 °C) for γ'-$(Ni_3Al)_{1-x}Fe_x$ ($L1_2$) alloys ($x \leq 0.08$). A plot of thermodynamic activities vs alloy composition is given in Fig. 11. It was derived from an excess chemical potential plot (Fig. 12 from the original work [83]) through the trivial transformation

$$a_i = x_i \exp\left(\frac{\mu_i^{\mathrm{E}}}{RT}\right), \tag{1}$$

where a_i is the activity and μ_i^{E} is the excess chemical potential of component i.

3.2. Ab initio

In this section are presented first principle calculations on the ternary system. There exists, of course, several publications concerned with one of the limiting binary systems, but there are only a few ab initio calculations of formation energies of structures in the Fe–Ni–Al system. Most of the available ab initio calculations in the Fe–Ni–Al system were performed in order to investigate the site preferences of alloying elements into one of the binaries. For this type of application, see Section 4.1.2.

Lechermann et al. [84] provided energies for both bcc and fcc ordered structures. The new Stuttgart ab initio mixed-basis pseudopotential code [85] in the generalised gradient approximation (GGA) was used to determine the energetics in the ground state.

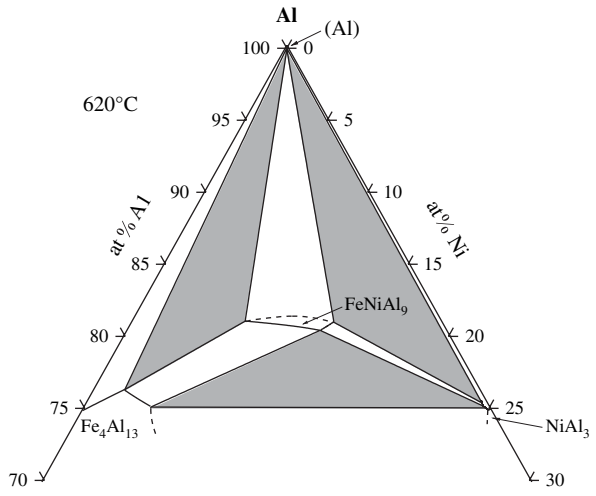

Fig. 9. Al-rich corner of the Fe–Ni–Al phase diagram at 620 °C [14,75].

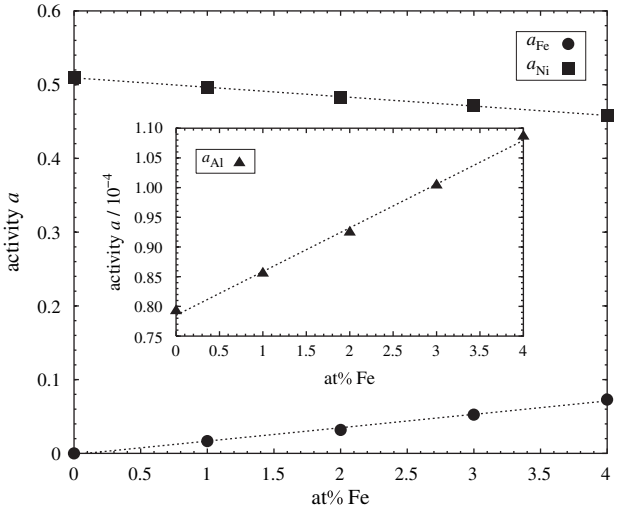

Fig. 11. Activities of Fe, Ni, and Al at 1473 K (1200 °C) in the γ'-Ni_3Al ($L1_2$) phase, with stoichiometry given by $Fe_x(Ni_3Al)_{1-x}$, according to Albers et al. [83]. Reference state: fcc Fe, fcc Ni, and liquid Al at 1473 K. The original work gives the excess chemical potential in the function of the alloy composition.

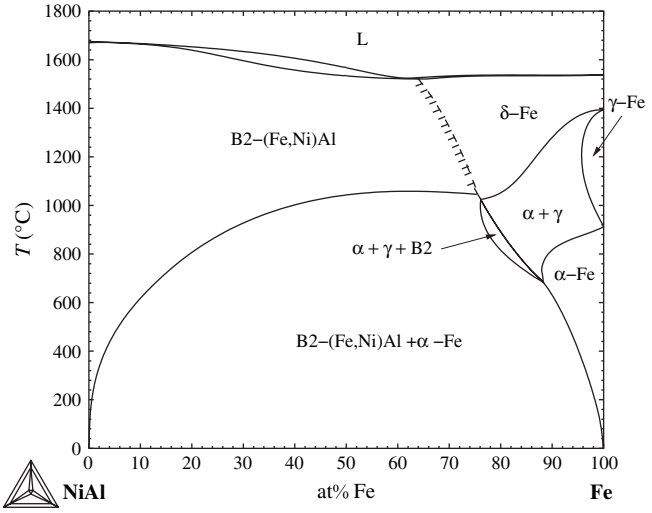

Fig. 12. Calculated isopleth from the NiAl side to the Fe corner of the Fe–Ni–Al phase diagram (to be compared with Fig. 7a).

Interatomic potentials were provided by Vailhe and Farkas [86] for a ternary B2 alloy with stoichiometry given by Ni–35Al–12Fe. The method employed was the Embedded Atom Method.[2] The potentials were subsequently used to simulate (100) screw dislocations.

4. Atomistic and diffusion data

4.1. Site occupancies

Site substitution of ternary elements in ordered compounds influences the electronic structure and consequently the properties, for instance, magnetic susceptibility and high-temperature resistance [87,88]. It is therefore essential to present site occupancy data in the present assessment.

4.1.1. Experimental

Site distributions of Fe in B2-ordered NiAl were measured by Anderson et al. [88] using the ALCHEMI (atom location by channelling-enhanced microanalysis) method in alloys with up to 10 at% Fe. A comparison with older investigations is done in the same work. The samples were first homogenised at 1300 °C for 5 h and then heat-treated at 800 °C for 72 h and water-quenched. The results indicate that Fe tends to occupy preferentially the stoichiometrically deficient sublattice (e.g. the Al sublattice in a $Fe_xNi_{50}Al_{50-x}$ alloy). The results of Goldberg and Shevakin [89] confirm this behaviour. However, part of the Fe atoms partition equally in both sublattices, generating Ni-site vacancies or Ni anti-site defects in the Al sublattice. The concentration of point defects increases with the Fe concentration, as also confirmed by Sprengel and Schaefer [90]. Time differential dilatometry experiments performed by these authors indicate a high structural vacancy concentration in $Fe_{10}Ni_{40}Al_{50}$ alloys.

Banerjee et al. [91,92] also applied the ALCHEMI method on several B2-FeAl and B2-NiAl alloys with ternary additions (Ti, V, Cr, Mn, Co, Ni, Cu). Three ternary alloys in the Fe–Ni–Al system were investigated, namely, $Fe_{50}Ni_{10}Al_{40}$, $Fe_{10}Ni_{50}Al_{40}$, and $Fe_{30}Ni_{25}Al_{45}$. It is apparent that Ni prefers the Fe sublattice in the $Fe_{50}Ni_{10}Al_{40}$ alloy, while Fe occupies preferentially the Al sublattice in $Fe_{10}Ni_{50}Al_{40}$. The last result confirms the behaviour described in the last paragraph. On the other hand, they show that Ni has an opposite effect on B2-FeAl.

Pike et al. [93] investigated site occupancies and vacancy concentrations over wide composition and temperature ranges within the single phase B2 field. Structural vacancies at all Al-rich samples were found, supporting the triple defect structure for the ternary alloys, and not only for the end-members B2-NiAl and B2-FeAl. For low Al concentrations, the results confirm that Fe anti-site defects are more stable than Ni ones.

4.1.2. Ab initio

Several ab initio calculations—as well as experimental investigations—are concerned with site occupancies and vacancy formation in the B2 structure [87,94–98]. Most results tend to confirm the experimental evidence at least qualitatively. Bozzolo et al. [98] used the Bozzolo–Ferrante–Smith (BFS) method [99] to calculate site preference of ternary additions to several binary B2 structures, among them Fe to NiAl and Ni to FeAl.

In Fu and Zou [94] calculations, Fe atoms occupy exclusively the Ni sublattice in Al-rich NiAl alloys. For Ni-rich NiAl alloys, the partition of Fe atoms varies with composition and temperature, due to the fact that the formation enthalpy of Fe defects in Ni and in Al sublattices is very small (<0.1 eV, with a preference for Fe at 0 K).

4.2. Diffusion-related properties

Due to the virtual interface formation, typically found in diffusion couples within the B2 phase region in aluminides [100], it is very difficult to determine diffusion coefficients for this structure. The problem arises from the diffusion mechanism in the ordered B2 phase [101] and is related to the presence of structural vacancies for off-stoichiometric compositions [102]. The difficulty seems to be more pronounced in the binary Ni–Al system, for diffusion couples with end-members at opposite sides of the equiatomic composition [100]. For the B2 structure in the Fe–Al system, the appearance of a pseudo-interface within the B2 phase field has not been reported, probably because the Fe–50 at% Al composition is very close to the extremity of the B2-stability range in this system [36].

Nevertheless, some early works have provided interdiffusion coefficients at 1000 °C or 1004 °C obtained by diffusion couple experiments with both end-members within the B2 stability range [103] or with fcc-FeNi (A1) against a B2 composition [104,105]. These data were later employed as input for a Calphad modelling of diffusion data [106,107]. The model in

[2] Though not exactly an ab initio method, this section was considered to be the best to accommodate this reference.

question proved to give satisfactory predictions on diffusion in the B2 phase field of the Al–Fe–Ni system.

Still within the B2 phase field, the so-called zero-flux plane (where the inter-diffusivity of a component vanishes within a single phase field) has been reported by Dayananda [108]. Interdiffusion coefficients in relation to observed double-serpentine diffusion paths were also investigated [109,110].

Ni and Fe tracer diffusion experiments were performed by Divinski et al. [111] for an $Fe_{10}Ni_{40}Al_{50}$ alloy from 1150 to 1550 K, corresponding to the B2 phase field. It was shown that the Fe diffusivity was 3–5 times higher than for Ni, but the presence of Fe decreases the activation energy for Ni diffusion when compared to stoichiometric NiAl [111]. The authors concluded that nearest-neighbour jumps, most probably by triple defect coupling, are the dominant diffusion mechanisms at these compositions.

For binary Fe–Al alloys with compositions around 25 at% Al, Ni tracer diffusivities were determined for A2 and B2 phases [112]. The results show a very weak dependence of the ordering reaction A2/B2 on the diffusivities in Fe_3Al. This result was also confirmed by Peteline et al. [113] for Fe-27 at% Al samples. It was also shown by Tokei et al. [112] that the diffusion process is controlled by mono-vacancies in the first-neighbourhood, both on the disordered and in the ordered case, and that Ni diffusion is much slower than for Fe, mainly because the Ni-site preferences. Due to the low-temperature stability range of the $D0_3$ phase, no data concerning diffusivity in this phase can be found in the literature.

The decrease of stability of the γ'-Ni_3Al ($L1_2$) phase with increasing Fe contents, i.e. (Al,Fe)Ni_3 alloys, as seen in Fig. 8, is associated with a decrease of the activation energy for ordering kinetics [114]. It has been found that this effect is related to a decrease in the vacancy formation energy with increasing Fe contents [115]. The vacancy migration energy shows no systematic dependence on the Fe concentration.

The dependence on the composition of the interdiffusion coefficients in binary Ni_3Al and ternary (Al,Fe)Ni_3 was investigated by Cermak et al. [116,117] in the $L1_2$ phase field at temperatures in the interval 1173–1533 K.

In order to study the stability of the interface between B2 and $L1_2$ diffusion couples in Ni–Al–X ternary alloys (X = Co, Cr, Cu, Fe, Mn, Mo, Nb, Si, Ta, Ti, V and W), Kainuma et al. [118] prepared several ternary Al–Ni–X diffusion couples in the temperature range from 1173 to 1573 K. It was found that, for the case of the Al–Fe–Ni system, the interface formed is a planar one. The authors related the stability of the interface to the partition behaviour of the alloying element X (in this case, Fe) in the B2/$L1_2$ equilibrium and to the diffusivities of X in the $L1_2$ phase.

The formation and growth of Fe-aluminide diffusion layers and the influence of ternary impurities have been investigated by Akdeniz and Mekhrabov [119]. The authors found a direct correlation between the effect of the ternary addition on the Al activity and the thickness of the diffusion layer. In the case of Ni, there is an increase in the Al activity, and consequently there is an increase in the diffusion layer when compared to "pure" Fe–Al.

5. Modelling

In this section, we are interested in the modelling of the Fe–Ni–Al phase diagram, following different methodologies. Calculations of other properties, such as formation energies or site occupancies, were given in Sections 3 and 4, respectively.

5.1. Calphad

There are very few direct Calphad-type modelling of the Al–Fe–Ni ternary system. The works that exist are usually restricted to one of the corners of the phase diagram.

Kaufman and Nesor [120] provided a first attempt in Calphad modelling of the Al–Fe–Ni system. Their results describe in general lines the part of the phase diagram close to the Fe–Ni binary system, for temperatures ranging from 927 °C to 1327 °C. One has to notice that the γ'-Ni_3Al ($L1_2$) phase was modelled as a binary compound, not allowing therefore any solubility of Fe.

The ordering in the bcc lattice was later studied by Ghosh et al. [121] who, besides experimental investigation of an alloy (solution treated at 1300 °C followed by water-quenching) with composition within the miscibility gap B2 + A2, performed a calculation of a vertical section very close to that shown in Fig. 7b. Their calculation predicts a large miscibility gap, as expected from the experiments, but its closing into a second-order reaction at a certain temperature (about 1000 °C, see Fig. 7b) was not reproduced by their model.

More recently, Jia et al. [71] presented a few experimental results on the γ-(Fe,Ni) → Ni_3Al ($L1_2$) transition near the Ni-rich corner, based on diffusion couples equilibrated from 900 °C to 1300 °C. The new results were then combined with the data from Bradley and Taylor [55] and further modelled following the Calphad approach. It is important to notice that the phase description employed by the authors considers the A2 and B2 and the A1 and the $L1_2$ as distinguished phases, contrary to the modern view on modelling of ordering reactions within the Calphad formalism [122,123]. Nevertheless, the results of Jia et al. [71] show a good agreement with the experimental data, and no doubt should be considered as a springboard to the modelling of the system, since it shows that, adding only a few ternary parameters to the binary databases, a good agreement with experimental evidence is immediately reached.

5.1.1. Additional calculations

Apart from published works, the same database employed for the calculation of the binary phase diagrams (see Section 2.1)—therefore containing binary interaction parameters only—was used by the present authors for calculations within the ternary Fe–Ni–Al phase diagram. In Fig. 5, a first result in the modelling of the solidus surface is shown, together with the experimental evidence, as already discussed in Section 2.3. It is seen that the introduction of a single ternary regular solution term L(Liquid, Fe, Ni, Al;0) = +60 kJ/mol already brings the calculation very close to the experimental data,

allowing us to draw the same conclusion as in the preceding paragraph.

In Fig. 12, another calculation using the preliminary database is shown. It is an isopleth from NiAl to the Fe corner, and should be compared with Fig. 7a. The calculation predicts a very narrow three-phase field A1 + A2 + B2 in this section. As discussed previously, these results disagree with the data of Dannöhl [65], but are in full agreement with experimental isothermal sections shown in Fig. 6a–g.

5.2. CVM calculations

The Fe–Ni–Al system has been subject to some CVM (Cluster Variation Method) [124] and BWG (Bragg–Williams–Gorsky)[3] [125–129] calculations. Since the investigators were mainly concerned with order/disorder transformations, all works are restricted to less than 50 at% Al and are usually limited to ordering in one of the base crystal structures, i.e. either bcc (A2, B2 and $D0_3$) or fcc (A1, $L1_0$ and $L1_2$), and more rarely with interactions between the two.

In the first place, it is worth mentioning the general work of Nishizawa et al. [130] on ternary ordering miscibility gaps. The work is intended as an analysis of the Bragg–Williams–Gorsky model as applied to ternary systems, and the influence of different interaction parameters on the morphology of the phase diagram. The model can be applied directly to the A2 + B2 miscibility gap in the Fe–Ni–Al system.

Shinoda et al. [131] analysed the stability of the B2 phase, connecting it to the free-energy minimum curves inside the ternary system, by means of the CVM in the irregular tetrahedron (IT) approximation [132]. The parameters for the calculations were obtained from heat of sublimation for the pure elements and alloy formation energies for the B2 phase [131].

In order to study the thermal concentration of vacancies, Shinoda et al. [133, 134] employed a slightly modified CVM approach to the Fe–Ni–Al plus vacancies system, applied to the B2 structure [133] in the bcc lattice and to the $L1_2$ structure [134] in the fcc lattice (only for the binary Ni–Al in this last case). The authors show successfully that the vacancy concentration in function of the Fe content in the B2 phase is in good agreement with experimental Fe interdiffusion coefficients [103].

The $D0_3$ + B2 phase relationship at 427 °C (700 K) was investigated by Gang and Yuanming [135] using the IT-CVM approximation. It was found that the two-phase field extends widely into the ternary system (up to ≈80 at% Ni), starting as a second-order reaction at the Fe–Al binary. However, only binary interaction parameters were used in the calculations.

Ordering in the bcc and fcc lattices was investigated by Lechermann et al. [84]. The interaction parameters for both lattices were taken from ab initio results and adjusted to the CVM tetrahedron approximation. The resulting phase diagrams—both the limiting binaries and the isothermal sections—show a shift in the temperature scale so that, for comparison with experimental results, the calculated temperatures have to be approximately halved. That only qualitative comparisons are possible is a very common problem when first-principles data are employed in CVM calculations [136]. Nevertheless, the general features of the equilibria between the A2 and B2 phases, and specially among the A1, B2 and $L1_2$ phases, are well described.

[3] Which is basically the simplest case of the CVM formalism.

6. Summary and conclusions

The available experimental data from the literature on the Fe–Ni–Al system were reviewed, consisting of phase relationships and phase boundaries in the ternary system and thermochemical and diffusion (both experimental and ab initio) data. The equilibrium between γ'-Ni_3Al and γ-(Fe,Ni) is a part of the phase diagram that still needs critical experimental evaluation to overcome the discrepancy in the available literature. The Al-rich corner of the ternary is also lacking more substantial information, mainly regarding the solidus/liquidus surfaces.

There are also only a few works concerned with thermodynamic measurements in the ternary system. On the other hand, there exist several investigations on site preferences, both experimental and ab initio, but they are mainly—or exclusively—interested in site occupancy in the B2 ordered structure. Also several papers on diffusion-related properties are found in the literature. Since the $D0_3$-Fe_3Al structure has a high technological appeal, it would be interesting to have more information about site occupancy in this structure.

The present status of the modelling of the system, following the Calphad and the CVM formalism, was briefly reviewed. In the case of Calphad modelling, the present status of the binary databases seems to indicate a good starting point for a thermodynamic description of the ternary system.

Acknowledgements

The authors would like to thank Prof. Bo Sundman for providing the databases for the calculations performed in the present work, and also for the help in the understanding of the models employed. Many thanks also to the COST-535 committee for providing funds to a Short Term Scientific Mission for Mr. Eleno to Stockholm and the ensuing discussions with Dr. Karin Frisk. Finally, thanks to Dr. Jacques Lacaze, Dr. Gabriele Cacciamani and Dr. Martin Palm for helpful discussions.

References

[1] Sauthoff G. Intermetallics. Weinheim, Germany: VCH; 1995.
[2] Sauthoff G. Intermetallics 2000;8:1101.
[3] Letzig D, Klöwer J, Sauthoff G. Z Metallkd 1999;90:712.
[4] Kainuma R, Ono N, Ishida. Mat Res Soc Symp Proc 1995;360:467.
[5] Ishida K, Kainuma R, Ohtani H, Nishizawa T. Mechanical Properties and Phase Transformations of Multi-Phase Intermetallic Alloys. The Minerals & Materials Society; 1995. 77–90.

[6] Kainuma R, Nakano H, Oikawa K, Ishida K, Nishizawa T. Mat Res Soc Symp Proc 1992;246:403.
[7] Marcon G, Lay S. Ann Chim Sci Mat 2000;25:21.
[8] Hao SM, Ishida K, Nishizawa T. Metall Trans A 1985;16:179.
[9] Marcon G, Peffen R, Lemaire H. IEEE Trans Magn 1978;14:685.
[10] Bitterlich H, Löser W, Schultz L. J Phase Equilib 2002;23:301.
[11] Rablbauer R, Frommeyer G, Stein F. Mat Sci Eng A 2003;343:301.
[12] Rivlin VG, Raynor GV. Int Met Rev 1980;25:79.
[13] Raynor G, Rivlin V. Phase equilibria in iron ternary alloys, chapter Al–Fe–Ni. London: The Institute of Metals; 1988. pp 107–121.
[14] Budberg P, Prince A. Ternary alloys. Weinheim: VCH; 1992. pp. 309–323.
[15] Raghavan V. J Phase Equilib 2005;26:70.
[16] Raghavan V. J Phase Equilib 1994;15:411.
[17] Hilpert K, Kobertz D, Venugopal V, Miller M, Gerads H. Z Naturforsch 1987;42:1327.
[18] Prince A. Bull Alloy Phase Diagrams 1981;2:149.
[19] Buschow KHJ, van Engen PG, Jongebreur R. J Magn Magn Mat 1983;38:1.
[20] Popiel E, Tuszynski M, Zarek W, Rendecki T. J Less-Common Met 1989;146:127.
[21] van der Kraan A, Buschow K. Physica 1986;138:55.
[22] Corby R, Black P. Acta Crystallogr B 1973;29:2669.
[23] Grin J, Burkhardt U, Ellner M, Peters K. Z Kristallogr 1994;209:479.
[24] Ellner M, Kolatschek K, Predel B. J Less-Common Met 1991;170:171.
[25] Hara Y, O'Handley RC, Grant NJ. J Magn Magn Mat 1986;54/57:1077.
[26] Ellner M, Kattner U, Predel B. J Less-Common Met 1982;87:305.
[27] Bradley AJ, Taylor A. Philos Mag 1937;23:1049.
[28] Tonejc A, Rocak D, Bonefacic A. Acta Metall 1971;19:311.
[29] Dumpich G, Wassermann EF, Manns V, Keune W, Murayama S, Miyako Y. J Magn Magn Mat 1987;67:55.
[30] Lutts A, Gielen PM. Phys Status Solidi 1970;41:K81.
[31] Khaidar M, Allibert CH, Driole J. Z Metallkd 1982;73:433.
[32] Lemmerz U, Grushko B, Freiburg C, Jansen M. Phil Mag Lett 1994;69:141.
[33] Grushko B, Lemmerz U, Fischer K, Freiburg C. Phys Status Solidi A 1996;155:17.
[34] Lemmerz U. Ber Forschungszent Juelich 1996;Juel-3243:124.
[35] Massalski TB, editor. Binary alloy phase diagrams. Metals Park (OH), USA: ASM International; 1991.
[36] Kattner UR. Binary Alloy Phase Diagrams. Metals Park, OH (USA): ASM International; 1991. pp. 147–149.
[37] Kubaschewski O. Iron-binary phase diagrams. Berlin: Springer-Verlag; 1982.
[38] Ikeda O, Ohnuma I, Kainuma R, Ishida K. Intermetallics 2001;9:755.
[39] Taylor A, Jones RM. J Phys Chem Solids 1958;6:16.
[40] Palm M. J Alloy Compd 1997;252:192.
[41] Ducher R, Stein F, Viguier B, Palm M, Lacaze J. Z Metallkd 2003;94:396.
[42] Eumann M. PhD. thesis, Universität Aachen, Aachen, Germany 2002.
[43] Seierstein M. Thermochemical database for light metal alloys, volume 2, chapter system Al–Fe. Bruxelles: European Comission; 1998. pp. 34–39.
[44] Ohnuma I, Kainuma R, Ishida K. CALPHAD and alloy thermodynamics. In: Turchi PEA, Gonis A, Shull RD, editors. Seattle (USA): TMS; 2002. p. 61–78.
[45] Singleton MF, Murray JL, Nash P. Binary alloy phase diagrams. Metals Park, OH (USA): ASM International; 1991. pp. 181–184.
[46] Ansara I, Dupin N, Lukas HL, Sundman B. J Alloy Compd 1997;247:20.
[47] Dupin N, Ansara I, Sundman B. Calphad 2001;25:279.
[48] Bremer FJ, Beyss M, Karthaus EK, Hellwig A, Schober T, Welter JM, Wenzel H. J Cryst Growth 1988;87:185.
[49] Ellner M, Kek S, Predel B. J Less-Common Met 1989;154:207.
[50] Swartzendruber LJ, Itkin VP, Alcock CB. Binary alloy phase diagrams. Metals Park, OH (USA): ASM International; 1991. pp. 1735–1738.
[51] Dinsdale A., Chart T. M.T.D.S.N.P.L. 1986, unpublished.
[52] Ansara I. 1987, unpublished.
[53] Lee BJ. Calphad 1993;17:251.
[54] Ellner M, Röhrer T. Z Metallkd 1990;81:847.
[55] Bradley AJ, Taylor A. P Roy Soc Lond A 1938;166:353.
[56] Döblinger M, Wittman R, Grushko B. J Alloy Compd 2003;360:162.
[57] Weidner E, Lei JL, Frey F, Wang R, Grushko B. J Alloy Compd 2002;242:156.
[58] Grushko B, Velikanova TY. J Alloy Compd 2004;367:58.
[59] de Laissardiere GT, Nguyen-Manh D, Mayou D. Prog Mater Sci 2005;50:679.
[60] Bradley AJ. J Iron Steel I 1949;163:19.
[61] Phillips HWL. J Inst Met 1942;68:27.
[62] Hao SM, Takayama T, Ishida K, Nishizawa T. Metall Trans A 1984;15:1819.
[63] Bradley AJ. J Iron Steel I 1951;168:233.
[64] Liu TF, Jeng SC, Wu CC. Metall Trans A 1992;23:1395.
[65] Dannöhl W. Arch Eisenhüttenwes 1942;15:321.
[66] Bradley AJ. J Iron Steel I 1952;181:41.
[67] Masahashi N, Kawazoe HH, Takasugi T, Izumi O. Z Metallkd 1987;78:788.
[68] Povarova KB, Filin SA, Maslenkov SB. Russ Metall 1993;1:156.
[69] Jia CC, Ishida K, Nishizawa T. Metall Mater Trans A 1994;25:473.
[70] Goman'kov VI, Tret'yakova SM, Monastyrskaya EV, Fykin LE. Russ Metall 1998;6:125.
[71] Jia C, Ishida K, Nishizawa T. J Univ Sci Technol Beijing 2000;7:277.
[72] Himuro Y, Tanaka Y, Kamiya N, Ohnuma I, Kainuma R, Ishida K. Intermetallics 2004;12:635.
[73] Himuro Y, Tanaka Y, Ohnuma I, Kainuma R, Ishida K. Intermetallics 2005;13:620.
[74] Ma Y, Ardell AJ. Z Metallkd 2003;94:972.
[75] Schrader A, Hanemann H. Aluminium 1943;25:339.
[76] Raj D, Bencze L, Kath D, Oates WA, Herrmann J, Singheiser L, Hilpert K. Intermetallics 2003;11:1119.
[77] Bencze L, Raj DD, Kath D, Oates WA, Singheiser L, Hilpert K. Metall Mater Trans B 2004;35:867.
[78] Grün A, Henig ET, Sommer F. Materialwiss. Grundlagen Symp. 7. Werkstoffwoche; 1996. 95–100.
[79] Breuer J, Grün A, Sommer F, Mittemeijer EJ. Metall Mater Trans B 2001;32:913.
[80] Zubkov AA, Emel'yanenko LP, Ul'yanov VI. Russ Metall 1993;3:35.
[81] Li G, Inoue R, Suito H. Steel Res 1996;67:528.
[82] Ostrovskii OI, Myasnikov VV, Ploshkin VV, Stomakhin AY, Grigoryan VA. Steel USSR 1976;6:612.
[83] Albers M, Kath D, Hilpert K. Metall Mater Trans A 1996;27:3569.
[84] Lechermann F, Fähnle M, Sanchez JM. Intermetallics 2005;13:1096.
[85] Meyer B., Elsässer C., Lechermann F., Fähnle M. Fortran 90 program for mixed-basis-pseudopotential calculations for crystals 2005. Max-Planck-Institut für Metallforschung, Stuttgart, Germany; in press.
[86] Vailhe C, Farkas D. Mat Sci Eng A 1998;258:26.
[87] Song Y, Guo ZX, Yang R, Li D. Acta Mater 2001;49:1647.
[88] Anderson IM, Duncan AJ, Bentley J. Intermetallics 1999;7:1017.
[89] Goldberg D, Shevakin A. Intermetallics 1995;3:293.
[90] Sprengel W, Schaefer HE. Defect Diffus Forum 2001;194–199:397.
[91] Banerjee R, Amancherla S, Banerjee S, Fraser HL. Acta Mater 2002;50:633.
[92] Amancherla S, Banerjee R, Banerjee S, Fraser HL. Int J Refract Met H Mater 2000;18:245.
[93] Pike LM, Anderson IM, Liu CT, Chang YA. Acta Mater 2002;50:3859.
[94] Fu CL, Zou J. Acta Mater 1996;44:1471.
[95] Mekhrabov AO, Akdeniz MV. Acta Mater 1999;47:2067.
[96] Parlinski K, Jochym PT, Kozubski R, Oramus P. Intermetallics 2003;11:157.
[97] Robouch BV, Burattini E, Kisiel A, Suvorov AL, Zaluzhnyi AG. J Alloy Compd 2003;359:73.
[98] Bozzolo GH, Noebe RD, Amador C. Intermetallics 2002;10:149.
[99] Bozzolo G, Noebe RD, Honecy F. Intermetallics 1999;8:7.
[100] Kainuma R, Ikenoya H, Ohnuma I, Ishida K. Defect Diffus Forum 1997;143–147:425.
[101] Rennhofer M, Sepiol B, Löser W, Vogl G. Intermetallics 2003; 11:573.

[102] Krachler R, Ipser H. Phys Rev B 2004:70. 054113.
[103] Moyer TD, Dayananda MA. Metall Trans A 1976;7:1035.
[104] Cheng GH, Dayananda MA. Metall Trans A 1979;10:1415.
[105] Cheng GH, Dayananda MA. Metall Trans A 1979;10:1407.
[106] Helander T, Ågren J. Acta Mater 1999;47:1141.
[107] Helander T, Ågren J. Acta Mater 1999;11:3291.
[108] Dayananda MA. Mat Sci Eng A 1989;120–121:351.
[109] Dayananda MA. Solid State Phenom 2000;72:123.
[110] Sohn YH, Dayananda MA. Acta Mater 2000;48:1427.
[111] Divinski S, Kang YS, Löser W, Herzig C. Intermetallics 2004;12:511.
[112] Tokei Z, Bernardini J, Erdelyi G, Godeny I, Beke DL. Acta Mater 1998;46:4821.
[113] Peteline S, Nijokep EMT, Divinski S, Mehrer H. Defect Diffus Forum 2003;216–217:175.
[114] Kozubski R, Soltys J, Cadeville MC, Pierron-Bohnes V, Kim TH, Schwander P, Hahn JP, Morgiel J. Intermetallics 1993;1:139.
[115] Partyka E, Kozubski R. Intermetallics 2004;12:213.
[116] Cermak J, Gazda A, Rothova V. Intermetallics 2003;11:939.
[117] Cermak J, Rothova V. Acta Mater 2003;51:4411.
[118] Kainuma R, Ichinose M, Ohnuma I, Ishida K. Mat Sci Eng A 2001;312:168.
[119] Akdeniz MV, Mekhrabov AO. Acta Mater 1998;46:1185.
[120] Kaufman L, Nesor H. Metall Trans 1974;5:1623.
[121] Ghosh G, Olson GB, Kinkus TJ, Fine ME. Proceedings of the international conference on solid–solid phase transformations. Pittsburgh, PA (USA): TMS; 1994. pp. 359–364.
[122] Kusoffsky A, Dupin N, Sundman B. Calphad 2001;25:549.
[123] Ansara I, Chart TG, Fernándes-Guillermet A, Hayes FH, Kattner UR, Pettifor DG, Saunders N, Zeng K. Calphad 1997;21:171.
[124] Kikuchi R. Phys Rev 1951;81:988.
[125] Bragg WL, Williams EJ. P Roy Soc Lond A 1935;A151:540.
[126] Bragg WL, Williams EJ. P Roy Soc Lond A 1934;A145:699.
[127] Inden G. Z Metallkd 1975;66:577.
[128] Inden G. Z Metallkd 1975;66:648.
[129] Inden G. Z Metallkd 1977;68:529.
[130] Nishizawa T, Hao SM, Hasebe M, Ishida K. Acta Metall 1983;31:1403.
[131] Shinoda T, Mishima Y, Suzuki T. Mat Res Soc Symp Proc 1995; 364:573.
[132] Ackermann H, Inden G, Kikuchi R. Acta Metall 1989;37:1.
[133] Shinoda T, Hosoda H, Mishima Y. Mat Sci Eng A 1995;192–193:930.
[134] Shinoda T, Hosoda H, Mishima Y, Suzuki T. Mat Trans JIM 1992;33:698.
[135] Gang M, Yuanming X. Acta Metall Sin 2002;38:914.
[136] Colinet C. CALPHAD and alloy thermodynamics. In: Turchi EA, Gonis A, Shull RD, editors. Seattle: TMS; 2002. p. 21–52.